Loose Coupling Approach of CFD with a Free-Wake Panel Method for Rotorcraft Applications

Jaewon Lee*, Sejong Oh and Kwanjung Yee*****
Department of Aerospace Engineering, Pusan National University, Busan, Korea 609-735

Sanghun Kim* and Dong-ho Lee**
School of Mechanical and Aerospace Engineering, Seoul National University, Seoul, Korea 151-742

Abstract

As a first step toward a complete CFD-CSD coupling for helicopter rotor load analysis, the present study attempts to loosely couple a CFD code with a source-double panel method. The far-field wake effects were calculated by a time-marching free vortex wake method and were implemented into the CFD module via field velocity approach. Unlike the lifting line method, the air loads correction process is not trivial for the source-doublet panel method. The air loads correction process between the source-doublet method and CFD is newly suggested in this work and the computation results are validated against available data for well-known hovering flight conditions.

Key Word : Helicopter Rotor, Field Velocity Approach, Panel Method, CFD

Introduction

There are several flight conditions for which accurate prediction of air loads of helicopter rotor is not easily achievable when the aeroelastic effects are neglected such as in high speed forward flight and high thrust condition. When the helicopter operates in such flight conditions, the structural deformation due to aerodynamic loads become significant, resulting in the different trim condition and performance. Hence, the computed air loads without aeroelastic deformation usually do not show good correlation with experimental results. Accordingly, for accurate helicopter rotor analysis it is necessary to simultaneously consider structural deformation as well as aerodynamic analysis, known as CFD-CSD coupling. Recently, considerable improvements in air load prediction were demonstrated using a CFD-CSD coupling approach by Sitaraman et al. [1, 4], Datta et al. [2] and Potsdam et al. [3] for various flight conditions such as high forward speed flight, blade-vortex interaction and low forward speed flight. It was shown that aerodynamics, aeroelasticity and trim analysis are essential ingredients for improving the air load prediction in forward flight.

In the CFD-CSD coupling approach by Potsdam et el. [3], the comprehensive code is used for trim and structural deformation, while aerodynamic analysis depends entirely on CFD. In this approach, the tip vortex wake is directly captured by CFD and no additional wake model is necessary. However, it is computationally intensive because huge amount of computational grid points are required to cover the whole flow field. In the CFD-CSD coupling by Sitaraman et al

* Graduate Student
** Professor
*** Assistant Professor
E-mail : daedalus@pusan.ac.kr Tel: 051-510-2481 Fax: 051-513-3760

[1, 4]. and Datta et al. [2], CFD is employed for near-field aerodynamic analysis only and the tip vortex wake at the far-field is modeled by using the free-wake method incorporated in the comprehensive code. The induced velocities by the tip vortex wake are transferred to the CFD module via field velocity approach. Although this approach may have some limitation in handling the intensive blade-wake interaction, it is computationally more efficient in that CFD calculation is performed only for a single blade and the far-field wake effects are incorporated from external module. In the former approach, the fidelity of aerodynamic calculation in the comprehensive code has no effects on the overall accuracy of rotor air loads. However, this is not the case for the latter approach since the wake effects are directly fed into the CFD module. One disadvantage of lifting line method embodied in the comprehensive code is that it usually has some difficulty in modeling the rotor blade with complex geometry such as BERP.

As a first step toward CFD-CSD coupling, the present study attempts to loosely couple CFD module with a source-double panel method. In the present calculation, the far-field wake effects are fed into the CFD module via field velocity approach as in Sitaraman et al[1,4]. Since the source-double panel method can consider the thickness of the rotor blade and accurately represents the complex geometry, it is expected to yield better results when handling a complex shaped blade. Unlike in the lifting line method, the air loads correction process is not trivial for source-double panel method. The air loads correction process between the source-doublet method and CFD is newly suggested in the present study and the computational results are validated against available data for a well-known hovering flight condition.

Methodology

In the current framework, a panel method with a wake model is used for rotor trim analysis as well as to provide the wake effects for CFD code, while the CFD code yields an accurate air loads and performances of the rotor blade. The computational methods employed in the present study are briefly described as follows.

CFD Method

The governing differential equations are the Euler equations. For computational efficiency, an Euler solver is chosen for the CFD module this time but a Navier-Stokes solver can also be adopted with the same ease. The Euler equations can be written in a conservation law form in a generalized coordinate system as follows:

$$\partial_\tau \hat{Q} + \partial_\xi \hat{E} + \partial_\eta \hat{F} + \partial_\zeta \hat{G} = 0 \tag{1}$$

The coordinate system (x,y,z,t) is attached to the blade. The vector of the conserved quantities $\hat{Q}$ and the inviscid flux vectors $\hat{E}$, $\hat{F}$ and $\hat{G}$ are given by

$$\hat{Q} = \frac{1}{J}\begin{bmatrix} \rho \\ \rho u \\ \rho v \\ \rho w \\ e \end{bmatrix}, \hat{E} = \frac{1}{J}\begin{bmatrix} \rho U \\ \rho u U + \xi_x p \\ \rho v U + \xi_y p \\ \rho w U + \xi_z p \\ UH - \xi_t p \end{bmatrix}, \hat{F} = \frac{1}{J}\begin{bmatrix} \rho V \\ \rho u V + \eta_x p \\ \rho v V + \eta_y p \\ \rho w V + \eta_z p \\ VH - \eta_t p \end{bmatrix}, \hat{G} = \frac{1}{J}\begin{bmatrix} \rho W \\ \rho u W + \zeta_x p \\ \rho v W + \zeta_y p \\ \rho w W + \zeta_z p \\ WH - \zeta_t p \end{bmatrix}, \tag{2}$$

In these equation, $H=(e+p)$ and U, V and W are the contravariant velocity components defined for example, as $U=\xi_t+\xi_x u+\xi_y v+\xi_z w$. The cartesian velocity components are given by u, v and w in the x, y and z directions, respectively. Also, the density, pressure and total energy per unit volume are represented by ρ, p and e, respectively. Whereas the velocity and the length scales are non-dimensionalized by the characteristic velocity and length scales, given by the ambient sound speed a_∞ and the rotor blade chord c, the pressure p, density ρ and the energy e are non-dimensionalized by the free stream reference values p_∞/γ, ρ_∞ and $\rho_\infty a_\infty^2$, respectively. The quantities ζ_x, ζ_y, ζ_z, ζ_t, etc., are the coordinate transformation metrics, and J is the Jacobian of the

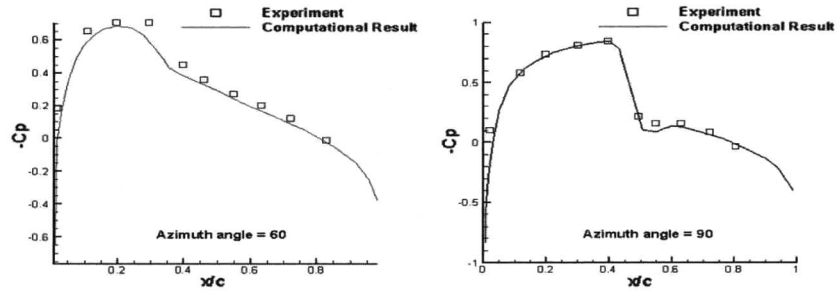

Fig. 1. C_p distribution of non lifting forward flight (r/R=0.9, M_{tip}=0.7, μ=0.3)

transformation. The fluid pressure p is related to the conserved flow quantities through the non-dimensional equation of state for a perfect gas given by

$$p=(\gamma-1)\left\{e-\frac{\rho}{2}(u^2+v^2+w^2)\right\} \tag{3}$$

Roe's flux difference method is employed for the spatial discretization of the convective flux terms. MUSCL interpolation with a flux limiter is used to obtain a higher order spatial accuracy. For temporal integration, the LU-SGS method has been employed. All boundary conditions are applied explicitly for computation efficiency.

For the validation of the CFD solver, a non-lifting forward flight case is calculated. The calculated results are shown in Fig. 1 are compared with the experimental results [5]. As shown in the figure, calculation results show good agreement with experimental results.

Panel Method with Free Wake Method for Trim Analysis

A unsteady source doublet panel method is used for trim analysis. For wake consideration, the time-marching free vortex wake model is coupled with the panel code. As well known, the free-vortex method offers relatively high fidelity and versatility at modest computational cost.

If the flow in the fluid region is considered to be incompressible and irrotational, then the continuity equation reduces to the Laplace's equation.

$$\nabla^2\Phi=0 \tag{4}$$

The general solution of Eq. (4) is given as a sum of source and doublet distribution over the body surface and its wake.

$$\Phi(\hat{P})=\frac{-1}{4\pi}\int_{body}\left[\sigma\left(\frac{1}{r}\right)-\mu\hat{n}\cdot\nabla\left(\frac{1}{r}\right)\right]ds+\frac{1}{4\pi}\int_{wake}\left[\mu\hat{n}\cdot\nabla\left(\frac{1}{r}\right)\right]ds+\Phi_\infty(\hat{P}) \tag{5}$$

Since Eq. (5) still does not uniquely describe a solution, the source distribution is set to be equal to the local kinematic velocity as in PMARC. The source strength becomes

$$\sigma=-\hat{n}\cdot\left(\overrightarrow{V_0}+\vec{v}\right) \tag{6}$$

In order to establish the boundary value problem, the local velocity at each panel on the body has to satisfy the zero flow condition normal to the body surface. Also, from the Kutta condition, the latest wake doublets are expressed in terms of the unknown surface doublets.

$$\mu_{wake}=\mu_{T.Eupper}-\mu_{T.E} \tag{7}$$

When specified at the body's collocation points, the boundary condition will have the form

$$[A_{ij}](\mu_k)=(RHS_k)=[B_{ij}](\sigma_k)+[C_i](\mu_{wk}) \tag{8}$$

This matrix has a nonzero diagonal and has a stable numerical solution. The resulting pressures can be computed by the Bernoulli equation.

The wake model is necessary to simulate the deformation of the wake. The free wake concept allows the vorticity to evolve in a free motion, and represents the physically correct approach to the unsteady aerodynamics. The time-marching free wake method is employed for the wake model. The wake is shed from the trailing edge line, and its size increases linearly with the time step.

In this paper, the wake doublet panel with constant strength is replaced by an equivalent vortex ring because it is known to become more efficient to calculate the induced velocity by the use of the Biot-Savart law. This approach is based on Hess [6], who showed that the constant strength doublet element is equivalent to a constant strength vortex ring placed along the panel edges. The singularity problem at the vortex center is resolved in producing a vortex core model. Vatitas's vortex model [7] is used to prevent vortex center singularity as suggested by Leishman, et al. [8] With Vatistas's vortex model, the equation for the induced velocity is modified into the form

$$\vec{V}=\frac{\Gamma}{2\pi}\frac{h}{\left(r_c^{2n}+h^{2n}\right)^{1/n}}\left(\cos\theta_1-\cos\theta_2\right)\hat{e} \tag{9}$$

where n is an integer.

The experimental results of Caradonna and Tung [9] are usually used as a validation case for hovering helicopter. The blade has an NACA0012 airfoil without twist and taper. For the hover simulation with time marching wake algorithm, the initial wake state is critical because the wake can become unstable owing to strong starting vortices generated by the impulsively starting blades. The initial instability was observed by many researchers and several ideas were suggested

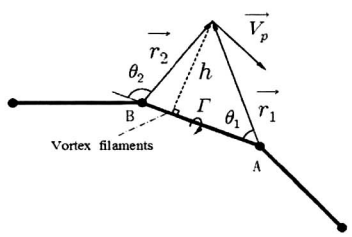

Fig. 2. Schematic showing the velocity induced by a straight-line vortex element

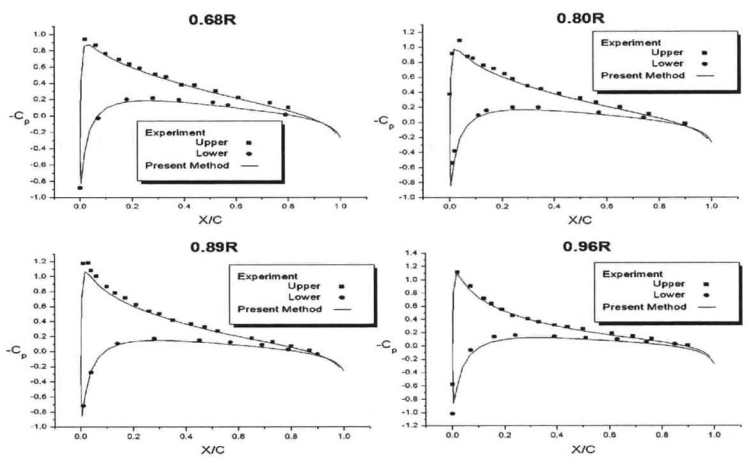

Fig. 3. C_p distribution at various radial sections(Mtip=0.439, θ_c=8°).

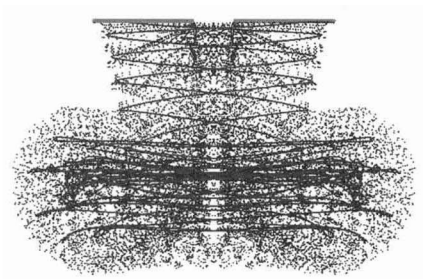

Fig. 4. Wake geometry of the hovering rotor (M_{tip}=0.439, θ_c=8°)

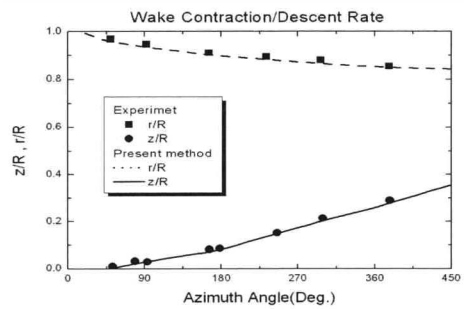

Fig. 5. Wake contraction/descent rate (M_{tip}=0.439, θ_c=8°)

to suppress the instability [10,11]. In the present work, a stable and correct solution could be obtained by using slow starting and simply imposing a growing law for the core radius of wake vortex filaments. The chordwise pressure distributions for a collective angle of 8° at the rotating speed of 1250 rpm, which corresponds to a tip Mach number of 0.439, are presented in Fig. 3.

Each blade has 44 panels in the chordwise direction and 22 panels in the spanwise direction. The computed pressures are shown to be in good agreement with the measurements. The geometry of the rotor and wake after 10 revolutions is shown in Fig. 4. The lines represent the tip vortex and the scattered points show the edge points of the inner wake panels. The trajectory of the tip vortices are also shown in Fig. 5.

Coupling Method

The coupling process between CFD and the panel method is summarized in Fig. 6.

A trim condition and the induced velocities obtained from the source-doublet panel with the free wake model are provided to the CFD module as a function of blade radius and azimuth angle. To impose the wake effect on the CFD module, the field velocity approach of J. D. Baeder et al. [12] is employed. The field velocity approach lies between the perturbation and surface transpiration method in terms of the computation time and the complexity of the algorithm. The induced velocity due to the vortical wake is included via time metric terms.

$$x_\tau \vec{i} + y_\tau \vec{j} + z_\tau \vec{k} = \vec{\Omega} \times \vec{r} - \overrightarrow{V_\infty} \tag{10}$$

where V_∞ is the wake-induced velocity.

After receiving the trim condition and the induced velocities, the CFD module iterates until periodicity in the air loads is obtained. Then the surface pressure distributions are sent back to the panel code as a function of radius and azimuth angle again. The panel method restarts calculation using the newly adjusted air loads.

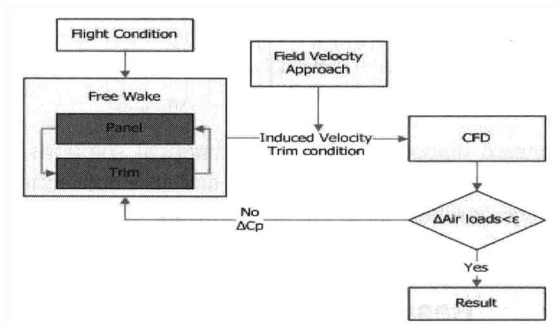

Fig. 6. Flow Chart of Coupling Method

Since the panel code is inherently incompressible, the pressure distribution transferred from the CFD code is converted to incompressible pressure coefficient by Prandtl-Glauert rule.

$$C_p = \frac{C_{p_0}}{\sqrt{1-M_\infty^2}} \tag{11}$$

The incompressible perturbation velocity in the chord direction is obtained from linearized pressure coefficient.

$$C_{p_0} = -\frac{2\bar{u}}{V_\infty} \tag{12}$$

The perturbation velocity components on the surface of a panel can be formulated as;

$$\bar{u} \cdot \hat{t} = \frac{1}{2\Delta l}(\mu_{k-1} - \mu_{k+1}) \tag{13}$$

The equation now has the form

$$\begin{pmatrix} 1 & -1 & 0 & 0 & \cdots & 0 & 0 & 0 \\ 1 & 0 & -1 & 0 & \cdots & 0 & 0 & 0 \\ 0 & 1 & 0 & -1 & \cdots & 0 & 0 & 0 \\ & & \ddots & \ddots & \ddots & & & \\ & & & \ddots & \ddots & \ddots & & \\ 0 & 0 & 0 & \cdots & 1 & 0 & -1 & 0 \\ 0 & 0 & 0 & \cdots & 0 & 1 & 0 & -1 \\ 0 & 0 & 0 & \cdots & 0 & 0 & 1 & -1 \end{pmatrix} \begin{pmatrix} \mu_1 \\ \mu_2 \\ \mu_3 \\ \vdots \\ \vdots \\ \mu_{n-2} \\ \mu_{n-1} \\ \mu_n \end{pmatrix} = \begin{pmatrix} \mu_{t1} \\ \mu_{t2} \\ \mu_{t3} \\ \vdots \\ \vdots \\ \mu_{t(n-2)} \\ \mu_{t(n-1)} \\ \mu_{tn} \end{pmatrix} \tag{14}$$

For a nonzero diagonal, the matrix is modified into the form

$$\begin{pmatrix} 1 & 0 & -1 & 0 & \cdots & 0 & 0 & 0 \\ 0 & 1 & 0 & -1 & \cdots & 0 & 0 & 0 \\ 0 & 0 & 1 & 0 & \cdots & 0 & 0 & 0 \\ & & \ddots & \ddots & \ddots & & & \\ & & & \ddots & \ddots & \ddots & & \\ 0 & 0 & 0 & \cdots & 0 & 1 & 0 & -1 \\ 0 & 0 & 0 & \cdots & 0 & 0 & 1 & -1 \\ 1 & -1 & 0 & \cdots & 0 & 0 & 0 & 0 \end{pmatrix} \begin{pmatrix} \mu_1 \\ \mu_2 \\ \mu_3 \\ \vdots \\ \vdots \\ \mu_{n-2} \\ \mu_{n-1} \\ \mu_n \end{pmatrix} = \begin{pmatrix} \mu_{t2} \\ \mu_{t3} \\ \mu_{t4} \\ \vdots \\ \vdots \\ \mu_{t(n-1)} \\ \mu_{tn} \\ \mu_{t1} \end{pmatrix} \tag{15}$$

However, the linear equations still cannot impose an unique solution since the diagonal element of the last low is zero. To solve the linear equations, the μ_n is set equal to the doublet strength from the panel code.

$$\begin{pmatrix} 1 & 0 & -1 & 0 & \cdots & 0 & 0 & 0 \\ 0 & 1 & 0 & -1 & \cdots & 0 & 0 & 0 \\ 0 & 0 & 1 & 0 & \cdots & 0 & 0 & 0 \\ & & \ddots & \ddots & \ddots & & & \\ & & & \ddots & \ddots & \ddots & & \\ 0 & 0 & 0 & \cdots & 0 & 1 & 0 & -1 \\ 0 & 0 & 0 & \cdots & 0 & 0 & 1 & -1 \\ 0 & 0 & 0 & \cdots & 0 & 0 & 0 & 1 \end{pmatrix} \begin{pmatrix} \mu_1 \\ \mu_2 \\ \mu_3 \\ \vdots \\ \vdots \\ \mu_{n-2} \\ \mu_{n-1} \\ \mu_n \end{pmatrix} = \begin{pmatrix} \mu_{t2} \\ \mu_{t3} \\ \mu_{t4} \\ \vdots \\ \vdots \\ \mu_{t(n-1)} \\ \mu_{tn} \\ \mu_{n,panel} \end{pmatrix} \tag{16}$$

Now, the matrix has a nonzero diagonal and stable numerical solutions can be obtained. The air loads are now updated through the difference of the doublet distribution between the CFD and panel code. The iterations are repeated until the delta surface pressure distributions are converged within a given tolerance.

Results and Discussion

The present approach described above has been validated against well-known hovering

cases. Fig. 7 shows the blade surface grids of the rectangular rotor blade. Body-conforming, single block, three dimensional computational grids were constructed by stacking C-H type grid. The computational grid used for the rectangular blade has 161 grid points in the wrap-around (along the chord) direction, 61 points in the spanwise direction and 41 points in the normal direction.

At first, in order to validate the overall accuracy of the present approach, the numerical calculations were performed for hovering cases and the results are compared with the experimental data of Caradonna and Tung [9]. Fig. 8 depicts the C_p distributions at selected spanwise positions for M_{tip}=0.439 case. It is shown that the suction peak tends to be underpredicted at the inboard region(r/R=0.5) but at the outboard region(r/R= 0.89), the overall pressure coefficients are in good agreement with the experimental data. The converged thrust coefficient is within around 6% error with the experiment (see Table 1)

Fig. 9 shows pressure contours on the upper surface with respect to iteration. As can be found in Figs. 8 and 9, there is no significant change in the pressure contour after two iterations.

The C_p and pressure contours on the upper surface in a transonic speed (M_{tip}=0.877) are shown in Figs. 10 and 11. It is found that the compute results also show good correlation in the transonic region. The shock location is captured with good accuracy. Even in the transonic region, the aerodynamic forces are converged after two iterations. From the results shown, it is concluded that the present coupling procedure for the source-double panel code works well for both subsonic and transonic cases.

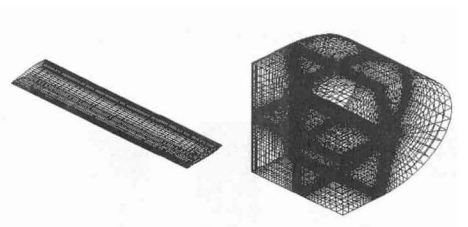

Fig. 7. Surface and Field Grids

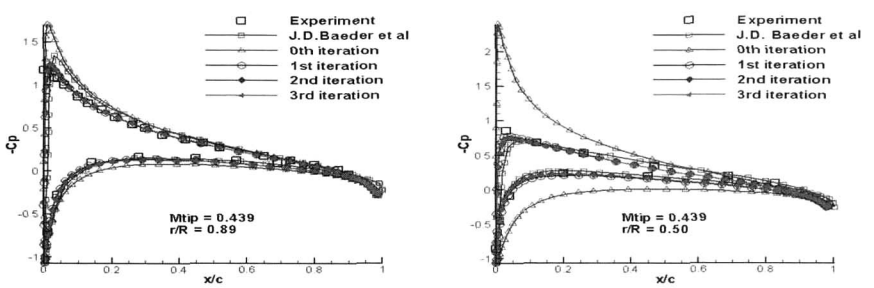

Fig. 8. C_p Distribution at r/R=0.50, 0.89 (M_{tip} = 0.439)

Table 1. CT comparison with experiment

	C_T (M_{tip}=0.439)	C_T (M_{tip}=0.877)
Experiment	0.00459	0.00473
0th iteration	0.009167	0.010030
1st iteration	0.004889	0.004836
2nd iteration	0.004891	0.005050
3rd iteration	0.004898	0.005033

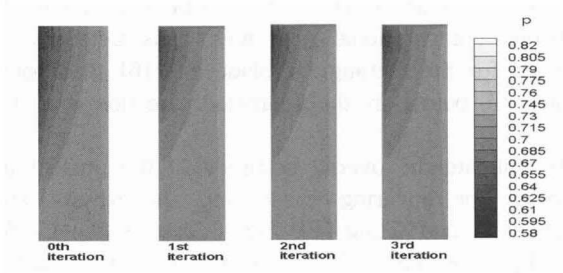

Fig. 9. Evolution of Pressure Contours with Iteration (M_{tip}=0.439)

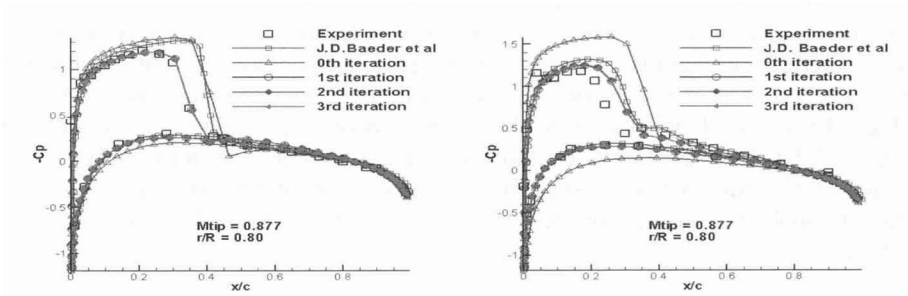

Fig. 10. C_p Distribution at r/R=0.80, 0.89 (M_{tip} = 0877)

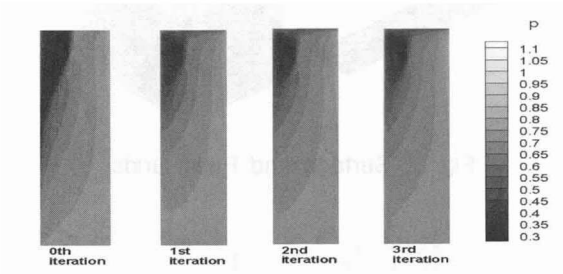

Fig. 11. Evolution of Pressure contours with Iteration (M_{tip}=0.877)

The C_p and pressure contours on the upper surface in a transonic speed (M_{tip}=0.877) are shown in Figs. 10 and 11. It is found that the compute results also show good correlation in the transonic region. The shock location is captured with good accuracy. Even in the transonic region, the aerodynamic forces are converged after two iterations. From the results shown, it is concluded that the present coupling procedure for the source-double panel code works well for both subsonic and transonic cases.

Conclusions

As a first step toward a complete CFD-CSD coupling, a CFD code has been coupled with a time-marching free wake model by using field velocity approach. To this end, the new coupling procedure is suggested to update the aerodynamic calculation between the CFD and source-doublet panel codes. The present procedure has been validated against the hovering cases for which experimental data are available and the following conclusions are reached.

1. The newly suggested coupling method between the CFD and panel codes is shown to work well for both subsonic and transonic regions.
2. For hovering cases, the present method is shown to yield reliable results for both

subsonic and transonic regions. The converged thrust coefficients are shown to be within about 6 % error compared to experimental data

3. It is shown that only 2~3 iterations between the CFD and panel codes are enough to obtain a converged solutions for hovering cases.

Acknowledgement

This work was supported by Grant No. R01-2005-10059-0 from the Basic Research Program of the Korea Science & Engineering Foundation.

References

1. J. Sitaraman, J. D. Baeder, I. Chopra : "Validation of UH-60A Rotor Blade Aerodynamic Characteristics Using CFD", *Proceeding of 59th Annual Forum of the American Helicopter Society*, Phoenix, Arizona, May 6~8, 2003.

2. A. Datta, J. Sitaraman, J. D. Baeder, I. Chopra, "Analysis Refinements for Prediction of Rotor vibratory Loads in High-Speed Forward Flight", *Proceeding of 60th Annual Forum of the American Helicopter Society*, Baltimore, MD, June 7~10, 2004.

3. M. Potsdam, H, Yeo, W. Johnson, "Rotor Airloads Prediction using Loose Aerodynamic/Structural Coupling", *Proceeding of 60th Annual Forum of the American Helicopter Society*, Baltimore, MD, June 7~10, 2004.

4. J. Sitaraman, A. Datta, J. D. Baeder, I. Chopra, "Coupled CFD/CSD Prediction of Rotor Aerodynamic and Structural Dynamic Loads for Three Critical Flight Conditions", *Proceeding of 31st European Rotorcraft Forum*, Florence, Italy, September 13~15, 2005.

5. D. A. Boxwell, F. H. Schmitz, W. R. Splettstoesser and K. J. Schultz, "Model Helicopter Rotor High Speed Impulsive Noise: Measured Acoustics and Blade Pressures", NASA TM 85850, 1983.

6. J. L. Hess, "Calculation of Potential Flow About Arbitrary Three-Dimensional Lifting Bodies", Final Technical Report MDC J5679-02, McDonnell Douglas, Long Beach, California, USA., 1972.

7. G. H. Vatistas, V. Kozel, and W. Mih, "A Simpler Model for Concentrated Vortices", *Experiments in Fluids*, Vol. 11, pp. 73-76., 1991.

8. J. G. Leishman, A. Baker and A. Coyne, "Measurements of Rotor Tip Vortices Using Three-component Laser Doppler Velocimetry", *Journal of the American Helicopter Society*, Vol. 41, No. 4, pp. 342-353, 1996.

9. F. X. Caradonna, C. Tung, "Experimental and Analytical Studies of a Model Helicopter Rotor in Hover", NASA Technical Memorandum 81232, TR-81-A-23, 1981.

10. K. Chung, S. Na, W. Jeon, and D. Lee, "Numerical Prediction of Rotor Tip-Vortex Roll-Up in Axial Flights by Using a Time-Marching Free-Wake Method", *KSAS International Journal*, Vol. 1. No. 1, pp. 1-12., 2000.

11. G. Quaranta, G. Bindolino, P. Masarati, and P. Mantegazza, "Toward a Computational Framework For Rotorcraft Multi-Physics Analysis: Adding Computational Aerodynamics To Multibody Rotor Models", *Proceeding of the 30th European Rotorcraft Forum*, Marseilles, France, Sep. 14-16, 2004.

12. H. Khanna, J.D. Baeder, "Coupled Free-Wake/CFD Solutions for Rotors in Hover Using a Field Velocity Approach", *Proceeding of 52nd Annual Forum of American Helicopter Society*, Washington D.C., June 4~6, 1996.